Post-print of: Bartmański M., Cieślik B., Głodowska J., Kalka P., Pawłowski Ł., Pieper M., Zieliński A.: Electrophoretic deposition (EPD) of nanohydroxyapatite - nanosilver coatings on Ti13Zr13Nb alloy. CERAMICS INTERNATIONAL. Vol. 43, iss. 15 (2017), p. 11820-11829. DOI: 10.1016/j.ceramint.2017.06.026

Electrophoretic deposition (EPD) of nanohydroxyapatite - nanosilver coatings on Ti13Zr13Nb alloy

Michal Bartmanski[a] Bartlomiej Cieslik[b], Joanna Glodowska[a], Pamela Kalka[a], Lukasz Pawlowski[a], Maja Pieper[a], Andrzej Zielinski[a]

[a] Gdansk University of Technology, Department of Materials Engineering and Bonding, Narutowicza 11/12, 80-233 Gdansk, Poland
[b] Gdansk University of Technology, Department of Analytical Chemistry, Narutowicza 11/12, 80-233 Gdansk, Poland

ABSTRACT

Titanium and its alloys are the biomaterials most frequently used in medical engineering, especially as parts of orthopedic and dental implants. The surfaces of titanium and its alloys are usually modified to improve their biocompatibility and bioactivity, for example, in connection with the deposition of hydroxyapatite coatings.

The objective of the present research was to elaborate the technology of electrophoretic deposition (EPD) of nanohydroxyapatite (nanoHAp) coatings decorated with silver nanoparticles (nanoAg) and to investigate the mechanical and chemical properties of these coatings as determined by EPD voltage and the presence of nanoAg. The deposition of nanoHAp was carried out at two voltage values, 15 and 30 V. The decoration of nanoHAp coatings with nanoAg was carried out using the EPD process at a voltage value of 60 V and a deposition time of 5 min. The thickness of the undecorated coatings was found to be 2.16 and 5.14 μm for applied EPD voltages of 15- and 30-V, respectively. The release rate of silver nanoparticles into an artificial saliva solution increased with exposure time and EPD voltage. The corrosion current, between 1 and 10 nA/cm^2, was significantly higher for undecorated nanoHAp coatings and close to that of the substrate for decorated nanoHAp coatings. The hardness of the undecorated nanoHAp coatings obtained at 15 and 30 V of EPD voltage attained 0.2245 ± 0.036 and 0.0661 ± 0.008 GPa, respectively. Resistance to nanoscratching was higher for thicker coatings. The wettability angle was lower for coatings decorated with nanoAg.

Keywords: Apatite D, Biomedical applications E, Films A, Nanocomposites B

1. Introduction

Titanium and its alloys have become the most popular materials for long-term load-bearing implants. For such materials, titanium of technical grades D and E (e.g. for dental implants or stents), made from the Ti6Al4V or Ti6Al7Nb alloy, is usually used. Titanium, which is characterized by weak mechanical properties, is suitable for small implants. The Ti6Al4V alloy has some disadvantages: its elastic modulus is much lower than that of bone, V may provoke adverse tissue reactions, and Al may initiate Alzheimer's disease [1,2]. The possible neuropathy and allergic reactions caused by Al, V, and Ni were also suggested [3]. Another study proved the non-toxicity of elements such as Ti, Zr, Ta and Nb [4]. In recent years, the Ti13Zr13Nb alloy, among the more than forty alloys investigated to date, seems to be the best candidate due to its non-toxicity and relatively low Young's modulus [5]. Nb and Zr are stabilizers of β-phase and cause a decrease of the Young's modulus so that the titanium Ti13Zr13Nb alloy is more biocompatible than others [6,7]. Moreover, the stable oxide TiO_2 film 1–4 nm thick is spontaneously formed on the surface the titanium Ti13Zr13Nb alloy. Its ability to natural self-passivation and presence of the titanium dioxide on the surface reduces the risk of migration of metal ions to body fluids after implantation [8].

The weak bonding of titanium and its alloys to bone and its lack of bioactivity have resulted in a great variety of different surface modification techniques, including acidic [9,10] and alkaline treatment, nanooxidation [11], micro- and nanopatterning [12], ion implantation [13], laser treatment [14], and deposition of phosphate coatings [15]. The deposition of phosphates, usually hydroxyapatite coatings, has recently been performed using techniques such as electrophoretic deposition (EPD) [16–22], electrochemically-assisted cathodic deposition (ECAD) [23–28], or both [29]; the sputtering technique [30–32]; hydrothermal deposition followed by electrochemical seeding [33]; chemical and thermal treatment [34]; the sol-gel method [35,36]; and biomimetic (chemical) deposition [18,37].

Nowadays, attempts are being made to deposit thin nanohydroxyapatite coatings, which are stronger, immediately adjacent to the

http://dx.doi.org/10.1016/j.ceramint.2017.06.026

substrate, and more resistant to brittle cracking, so that they can be recommended for covering, e.g., small screw dental implants. These thin coatings are prepared using the electrophoretic (EPD), electrocathodically-assisted (ECAD), or hydrothermal methods [16,38–42]. Dudek and Goryczka [21] obtained 2.4-μm HAp coatings on NiTi alloys using the EPD method. A extremely thin 300-nm bone-like apatite layer was created by HAp sputtering onto a Ti6Al4V alloy [30]. Using [43] the chemical method, HAp coatings 1.0–1.8 μm thick were deposited in a solution of $Ca(NO_3)_2{\cdot}4H_2O$, KH_2PO_4, KOH, and EDTA at 65–95 °C. According to [27], 10-μm-thick HAp layers were obtained using ECAD on a previously formed ZrO_2 layer in a mixed solution of $Ca(NO_3)_2$, $NH_4H_2PO_4$, and NaF. NanoHAp was also obtained using a combination of friction stir processing and EPD on a TiCaP layer [19]. The wire-brushing treatment was used to modify the EPD method, resulting in nanohydroxyapatite coatings.

Post-surgery treatment following implantation is carried out through the administration of antibiotics. Similar effects can be achieved via the addition of some nanometals, operating as biocidal agents, to the coating. Silver is usually applied directly to the implant surface as pure metal or nanosilver. The application of silver or nanosilver in phosphate coatings deposited by different methods has been exhaustively investigated [39,44–49]. Pang and Zhitomirsky [39] obtained nanocomposite coatings such as HAp-Ag-chitosan multilayers with thicknesses to 20 μm, as determined by deposition time. Mo et al. [44] produced a composite of Ag^+ ions and nanosized HAp with TiO_2, which was then deposited onto titanium using a dipping method. Chen et al. [45] prepared silver-containing hydroxyapatite coatings by means of co-precipitation or plasma spraying. Qu et al. [46] produced uniform Ag/HA composite coatings on the surfaces of porous Ti substrates using a sol-gel process. Grubova et al. [47], using radio frequency (RF) magnetron sputter deposition, obtained silver-containing hydroxyapatite coatings containing 0.13–0.36 wt% silver. Fu et al. [48] coated a titanium substrate with hydroxyapatite via electrochemical crystallization and then deposited silver nanoparticles via the electrochemical reduction of aqueous Ag^+ to Ag°. The quantity and size of silver nanoparticles were determined by the relevant ECAD time. Geng et al. [49] incorporated silver into calcium phosphate coatings on titanium using the hydrothermal method. Antibacterial effects were observed against *Staphylococcus aureus*, *Staphylococcus albus* and *Escherichia coli* in [44,46,47]. The key problem, which is seldom analyzed [45], is the content of silver in the coating and its distribution in such a way as to assure that the silver content in the surrounding body fluid is sufficiently high, at least during the primary fixation period, but does not exceed a lethal dose. In [31] coatings with varying Ag contents were deposited on Ti6Al4V alloy substrates via co-sputtering of hydroxyapatite, SiC, and Ag targets. The antibacterial efficiency of hydroxyapatite against Gram-positive bacteria was observed in the presence of silver. Hydroxyapatite with Ag content less than 1% demonstrated excellent resistance to bacterial attack. In [25] the electrodeposition method was used to prepare silver- and strontium-modified antibacterial HAp layers applied to TiO_2 nanotubes. Both Sr^{2+} and Ag^+ ions could be incorporated into the HA lattice to form SrAgHA coatings. The composite coatings were bioactive and opposed the growth of *Staphylococcus aureus* bacteria. In [50] a SrCuHAp coating was obtained. Cu was incorporated into HAp to improve its antimicrobial properties, in particular against *Escherichia coli*. A low contact angle value revealed the coating's hydrophilic nature.

Despite the existence of research on HAp-Ag, only a few papers have focused on nanoHAp-nanosilver coatings, not all of which used the Ti13Zr13Nb alloy as a substrate. Moreover, data on the release of silver from the coating during exposure to simulated body fluids are seldom included. The present research is focused on determination of the effects of both EPD voltage and the presence of nanosilver on the microstructure and physical, chemical, and mechanical properties of thin nanohydroxyapatite coatings characterized by particular suitability for dental implants.

Table 1
Chemical composition of the Ti13Nb13Zr alloy, wt%.

Element	Nb	Zr	Fe	C	N	O	Ti
wt%	13.0	13.0	0.05	0.04	0.019	0.11	remainder

2. Material and methods

2.1. Preparation of specimens

The Ti13Zr13Nb [51] alloy of the composition shown in Table 1 was used as a substrate. Specimens 4 mm in thickness and 15 mm in radius, cut from rods, were prepared. The surface roughness was adjusted to Ra 0.13 μm using SiC abrasive paper up to 2000 grit. Then the specimens were rinsed with isopropanol and ultrasonically cleaned (Sonic-3, Polsonic, Poland) in distilled water for 60 min, pickled in 25% HNO_3 for 10 min to remove oxide layers from the substrate [52], and finally rinsed thoroughly with distilled water prior to deposition.

2.2. Electrophoretic deposition of nanoHAp coatings

Electrophoretic deposition (EPD) was carried out in a suspension prepared by dispersing 0.1 g of HAp nanopowder in 100 mL of ethanol (anhydrous, 99.8% purity). The commercial HAp nanopowder (MKnano Canada) was characterized by an average particle size of about 20 nm. The suspensions were obtained via ultrasonic mixing for 60 min at room temperature. The Ti13Zr13Nb substrate was used as a cathode and platinum as a counter electrode. The electrodes were placed parallel to each other within a distance of 10 mm and connected to a DC power source (MCP/SPN110-01C, Shanghai MCP Corp., China). Electrophoretic deposition was performed at 15 or 30 V for 1 min at room temperature. Finally, the as-deposited coatings were air-dried at room temperature for 24 h.

2.3. Thermal treatment of nanoHAp coatings

The coated Ti13Zr13Nb specimens were thermally treated in a tubular furnace (Protherm PC442, Ankara, Turkey) in a vacuum at 800 °C for 120 min, after being heated from room temperature to 800 °C at a rate of 200 °C/h; subsequently, they were cooled to room temperature in the furnace.

2.4. Electrophoretic deposition of nanosilver

Nanohydroxyapatite coatings (later designated as nanoHAp-15V and nanoHAp-30V) applied to the Ti13Zr13Nb substrate were decorated with nanoAg using the EPD method. Commercial nanosilver powder (Hongwu International Group Ltd, China), with particles about 30 nm in size, was used. The deposition was carried out in suspensions prepared by dispersing 0.01 g of nanoAg powder in 100 mL of ethanol (anhydrous, 99.8% purity) and ultrasonic mixing for 60 min. A nanoHAp/Ti13Zr13Nb substrate and platinum foil were used as electrodes; these were placed parallel to each other within a distance of 10 mm and connected to a DC power source (MCP/SPN110-01C, Shanghai MCP Corp., China). The EPD was performed at 60 V for 5 min at room temperature. Finally, the as-decorated coatings (designated later as nanoHAp-15V/nanoAg and nanoHAp-30V/nanoAg) were air-dried at room temperature for 24 h.

2.5. Structure and morphology of nanoHAp and nanoHAp/nanoAg coatings

Surfaces and cross sections of the coatings were observed using a high-resolution scanning electron microscope (JEOL JSM-6480). The chemical composition of the coatings was investigated using an X-ray

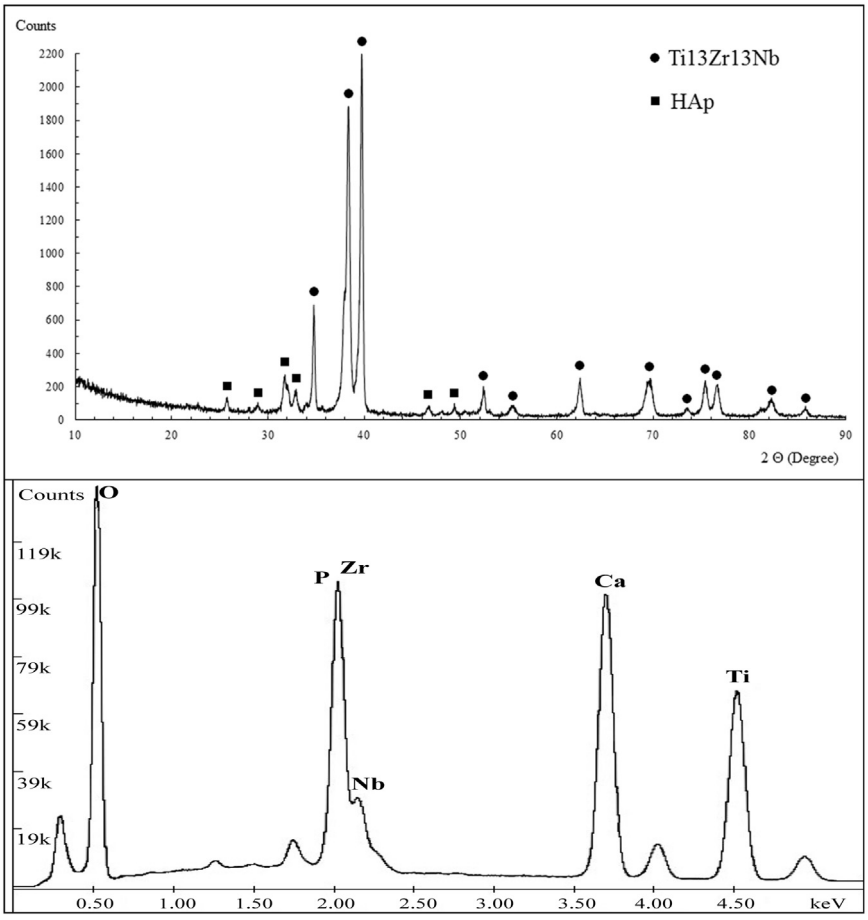

Fig. 1. XRD patterns (left) and EDS spectrum (right) of nanoHAp-30V coating.

energy-dispersive spectrometer (EDS), Edax Inc., USA. Phase identification was performed using an X-ray diffraction pattern (XRD Philips X'Pert Pro, Netherlands) with monochromatized CuKα radiation and a scan rate of 0.02°/s within a 2Θ range of 10–90°. An atomic force microscope (AFM, NaniteAFM) was applied to study the surface topography. The investigations were performed in the non-contact mode at a force of 55 mN. The roughness indexes Ra and Sa were estimated within an area of 80.4 × 80.4 μm.

2.6. Silver release in simulated body fluid (SBF) solution

The concentration of Ag ions was studied in solution following immersion of specimens of nanoHAp-15V/nanoAg and nanoHAp-30V/nanoAg in SBF for various periods (1, 3, and 7 days) at 38 °C. The content of Ag^+ ions was determined by a SensAA atomic absorption spectrometer (GBC Scientific Equipment Pty Ltd, Australia) with a dual beam optical system and air-acetylene flame atomization. A deuterium lamp was used for background correction; a silver hollow cathode lamp (0.4 mA) served as the radiation source. The wavelength used for Ag analysis was 328.1 nm, slit width 0.5 nm. The Ag standard solution for AAS, 1000 mg/L in 2% HNO_3 (VWR Chemicals), was applied to preparation of the calibration solution. The first standard solutions, at an average concentration of 10 mg/L, were prepared by diluting 1000 mg/L stock solutions. Six standard solutions were made for the calibration curve: 0.1, 0.3, 0.5, 1.0, 2.0, and 3.0 mg/L. The linear regression method was applied to the calibration curve.

2.7. Corrosion behavior of nanoHAp and nanoHAp/nanoAg coatings in SBF

The electrochemical measurements of corrosion parameters were made for nanoHAp-15V, nanoHAp-30V, nanoHAp-15/nanoAg, nanoHAp-30V/nanoAg, coated Ti13Zr13Nb alloy, and Ti13Zr13Nb alloy as a reference specimen, in a potentiodynamic mode in simulated body fluid (SBF) at room temperature. SBF was prepared according to PN-EN ISO 10993-15 [53] by dissolving reagent grade chemicals: $(NH_2)_2CO$ (0.13 gL^{-1}), NaCl (0.7 gL^{-1}), $NaHCO_3$ (1.5 gL^{-1}), Na_2HPO_4 (0.26 gL^{-1}), K_2HPO_4 (0.2 gL^{-1}), KSCN (0.33 gL^{-1}), KCl (1.2 gL^{-1}). A three-electrode cell setup was used with a standard platinum electrode as a counter and Ag/AgCl (saturated with potassium chloride KCl) as a reference electrode. All experiments were performed using a potentiostat/galvanostat (Atlas 0531, Atlas Sollich, Poland). Prior to the experiment, the samples were stabilized at their open circuit potential (OCP) for 5 min. A potentiodynamic polarization test was carried out at a potential change rate of 1 mV/s, within a scan range from –600–2000 mV. The corrosion potential (E_{corr}) and corrosion current density (i_{corr}) were determined from the polarization curves using the Tafel extrapolation method.

2.8. Nanomechanical studies

Nanoindentation tests were performed with a NanoTest Vantage (Micro Materials) using a Berkovich three-sided pyramidal diamond. The nanoHAp-15V and nanoHAp-30V coatings were tested, with 10

independent measurement tests for each sample. The maximum applied force was equal to 5 mN; the loading and unloading rates were set at 20 s; the dwell period at full load was 10 s. The distances between the subsequent indents were set at 50 μm. During the indent, the load-displacement curve was determined using the Oliver-Pharr method. From the load-penetration curves, surface hardness (H) and Young's modulus (E) were calculated using integrated software. In calculating Young's modulus (E), a Poisson's ratio of 0.3 was assumed for the HAp coating. Nanoscratch tests were performed with the NanoTestVantage (Micro Materials) using a Berkovich three-sided pyramidal diamond. Scratch tests were carried out by increasing the load from 0 to 200 mN, at a loading rate of 1.3 mN/s, at a distance of 500 μm. The adhesion of the coating was based on the change in frictional force during the test.

2.9. Contact angle studies

Water contact angle measurements were carried out for the Ti13Zr13Nb alloy, nanoHAp-15V, nanoHAp-30V, nanoHAp-15V/nanoAg, and nanoHAp-30V/nanoAg coatings using a contact angle goniometer (Zeiss, Germany) at room temperature. All measurements were repeated three times for each specimen.

3. Results and discussion

3.1. Structure and morphology of nanoHAp coatings

Fig. 1 illustrates the X-ray diffraction patterns for the nanoHAp-30V coating; the spectrum for the nanoHAp-15V coating was similar. For both nanoHAp coatings, the XRD pattern indicates the presence of peaks typical of hydroxyapatite [17], of crystalline HAp, and peaks of the titanium alloy Ti13Zr13Nb substrate [8]. As amorphous HAp phase may dissolve within days after implantation, in order to enhance the bioactivity of the implant material it is necessary to obtain crystalline HAp, which is similar to the biological apatite in natural human bone [54]. The peaks of hydroxyapatite phase are more intense for nanoHAp-30V than those of nanoHAp-15V, which can be attributed to the different thickness of the coating. The XRD patterns for the coated surface reveal peaks of the Ti13Zr13Nb substrate of very high intensity, due to the low thickness and density of nanoHAp coatings, which allows easy penetration of X-ray waves into the titanium alloy.

In the EDS spectra, the same elements (Ca and P for the coatings, and Ti, Zr, and Nb for the substrate) were detected for both coatings. The presence of the peaks originating from the titanium alloy substrate is especially pronounced in the presence of a thin coating (Fig. 1).

Fig. 2 shows the SEM images of the microstructure of the nanoHAp coatings following thermal treatment. Cracks appear on both types of coatings, in particular on nanoHAp-30V, on which a greater number of longer cracks are seen. Such cracks may occur due to water evaporation and the passage from amorphous to crystalline phase associated with shrinkage of the nanoHAp coating. NanoHAp coatings are composed of grain agglomerates separated by numerous pores. According to Boccaccini et al. [55], particles of HAp at relatively low electrochemical potential during EPD cannot properly migrate or produce a homogenous coating. The higher number of agglomerates observed in nanoHAp-30V is due to the more rapid kinetics of the migration process and reduced time in which to find and occupy the most suitable position for the formation of a uniform coating [56,57].

Fig. 3 shows the surface topography obtained by means of AFM for both nanoHAp coatings. The roughness of the coatings increases with increasing voltage due to the presence of a greater number of agglomerates on the surface. The roughness of coatings (Table 2) is typical of the EPD method. Surface roughness is responsible for cell interaction in the human body. The high level of surface roughness ensures better tissue adhesion and provides improved primary stabilization between an implant and bone [58,59]. Rough and porous coatings facilitate the adhesion of a greater number of osteoblasts and can stimulate production of the extracellular matrix [13,60].

Fig. 4 shows the thickness of coatings, with means assessed at 2.16 ± 0.49 μm for nanoHAp-15V coating and 5.14 ± 0.51 μm for nanoHAp-

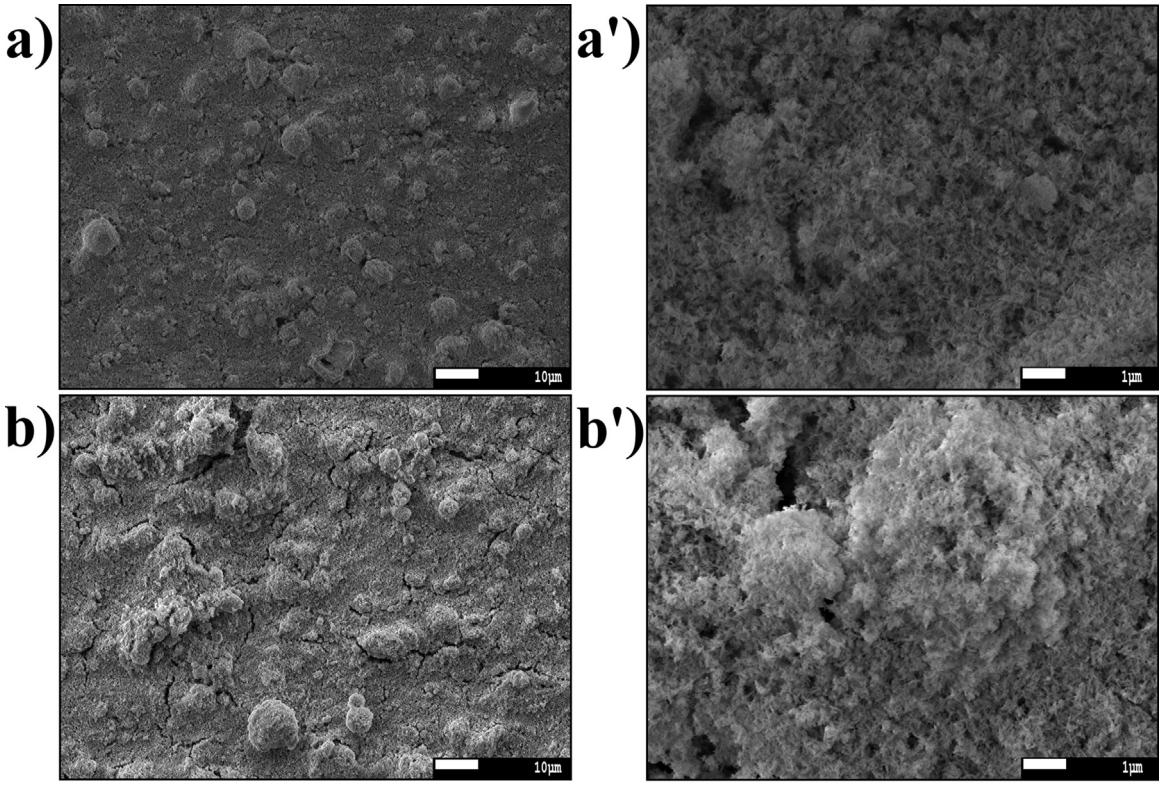

Fig. 2. SEM images of nanoHAp-15V (a, a′) and nanoHAp-30 V (b, b′) coatings.

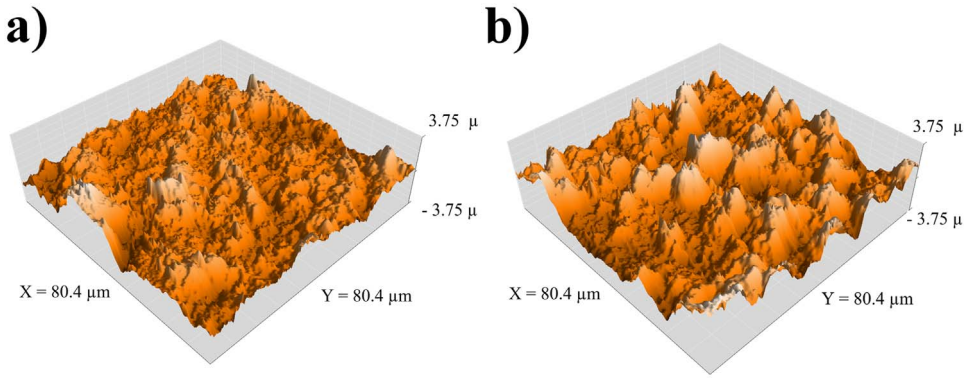

Fig. 3. Surface topography of nanoHAp-15V (a) and nanoHAp-30V (b) coatings within an area of 80.4 × 80.4 µm.

Table 2
Roughness parameters of the nanoHAp-15V and nanoHAp-30V coatings within an area of 80.4 × 80.4 µm.

Sample	R_a parameter (µm)	S_a parameter (µm)
nanoHAp-15V coating	0.51 ± 0.15	0.51
nanoHAp-30V coating	0.67 ± 0.15	0.73

30V. The coating thickness increases distinctly with EPD voltage in accordance with Coulomb's law. Goryczka et al. [21] showed that either deposition time or applied voltage could result in an increase in HAp coating thickness. Abdeltawab et al. [57] showed that, in the initial period of EPD at a constant voltage, thickness increased with time, but that over a longer period this effect was not observed; presumably, the EDP voltage might become more important. Here the thickness increases, even after a very short EDP time, more than twofold with doubled voltage. The cross sections also illustrate that both nanoHAp coatings are immediately adjacent to the Ti13Zr13Nb substrate, with no delamination.

3.2. Electrophoretic deposition of nanoAg on nanoHAp coatings

As shown in Fig. 5, nanosilver clusters decorate the surface of the nanoHAp coatings. The EDS spectra confirmed the presence of nanoAg on the surface of nanoHAp coatings. The effects of voltage used in the previous deposition of nanoHAp coatings and, subsequently, of surface topography on the deposition of nanosilver particles appear to be negligible. The clusters of nanosilver observed on the surface measure between 200 and 300 nm. The distribution of nanosilver particles over the surface is uniform.

3.3. Silver release in simulated body fluid (SBF) solution

The release of nanoAg from decorated nanoHAp coatings to SBF (Fig. 6) increases over time. The test temperature represents the temperature of inflammation in the human body. The results show that a significant number of Ag ions are released into the solution in such conditions, even during the first day. This may be caused by the oxidation of Ag as a reaction with water and the transition of Ag to ions [45]. There is a significant difference between the release of silver from nanoHAp-30V and nanoHAp-15V coatings. The roughness of the nanoHAp coating is likely the reason.

The decrease in the size of silver powder grains (up to about 30 nm) results in changes in physicochemical properties and above all in the increase in particle activity. Small size also confers greater particle mobility both in the environment and in the body [61,62]. Moreover, greater surface roughness of the nanoHAp-30V coating increases the possibility of proper location and attachment of the silver nanoparticles during the electrophoretic process.

Glover et al. proposed 3-stage model, with explained the formation of new nanoparticles. First nanosilver particles Ag° are attached to the substrate, next they adsorb the water layer (with Ag° changed to Ag^+) and as the last, nanosilver can properly migrate to the environment [63,64].

The release rate of nanoAg into SBF solution is closely correlated with the bactericidal and antibacterial properties of the decorated nanoHAp coating. The minimum required value of silver concentration with bactericidal effects is 0.1 ppm; the value of cytotoxic concentration of silver is 1.6 ppm [65]. Here, after one day of exposure, the free silver concentration in solution exceeds 0.1 ppm for nanoAg decorating nanoHAp-30V; in the case of a lower deposition voltage, this limit is achieved after 3 days. On the other hand, after 7 days of exposure, the concentration of silver is well below the cytotoxicity limit value.

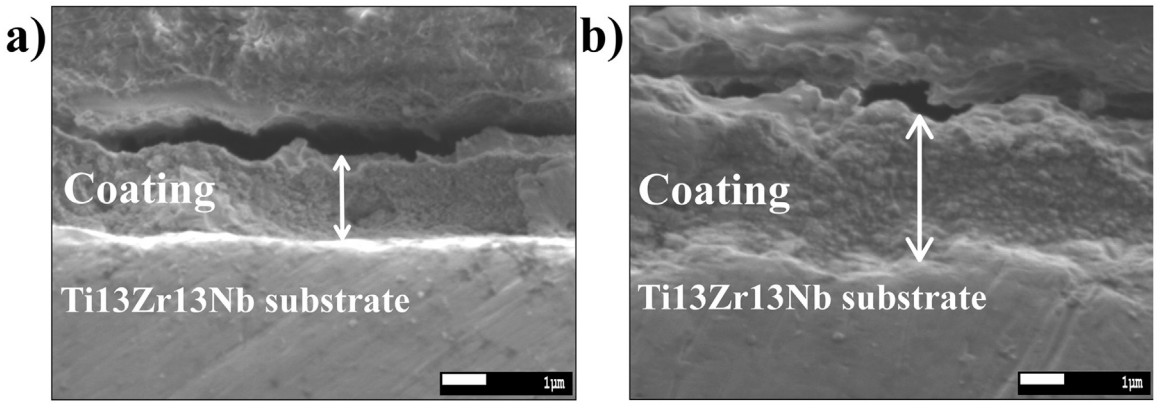

Fig. 4. Cross sections of nanoHAp-15V (a) and nanoHAp-30V (b) coatings following thermal treatment.

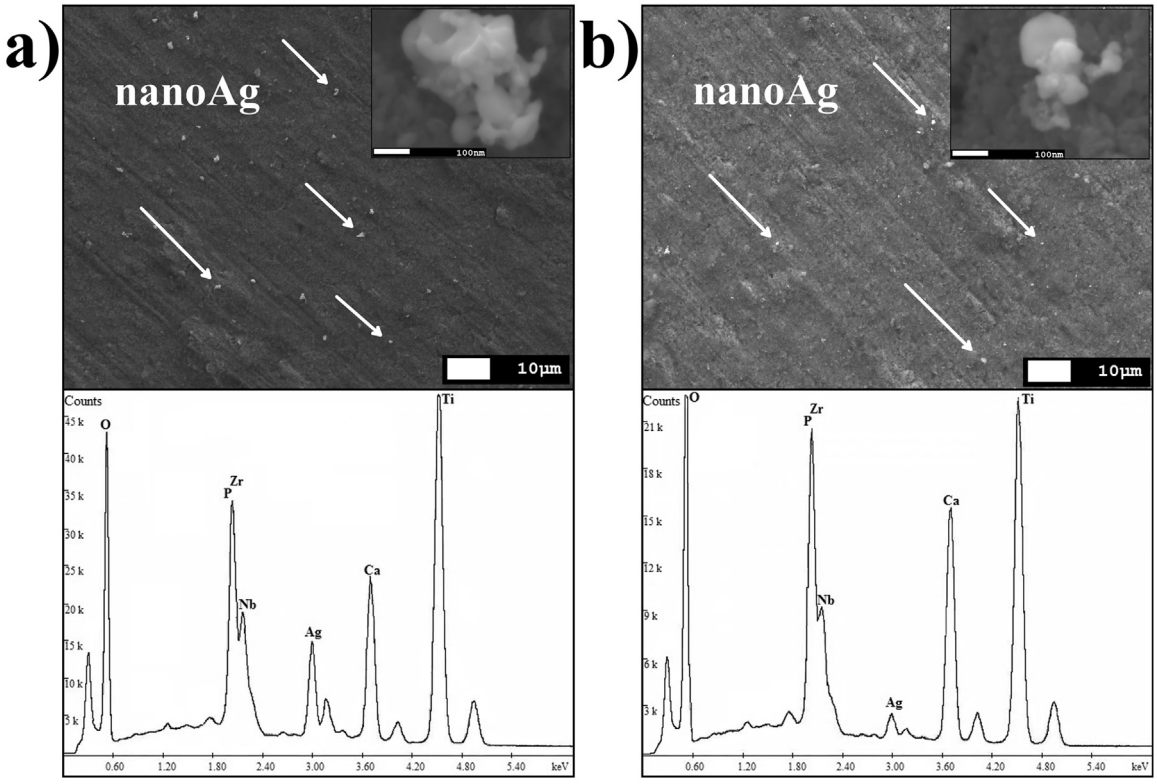

Fig. 5. SEM images (top) and EDS spectra (bottom) of nanoHAp-15V/nanoAg (a) and nanoHAp-30V/nanoAg (b) coatings.

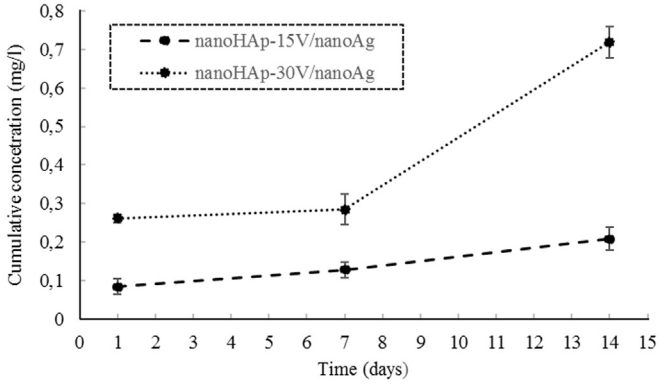

Fig. 6. Cumulative concentrations of Ag ions released from nanoHAp-15V/nanoAg and nanoHAp-30V/nanoAg after 1, 7, and 14 days exposure in SBF at 38 °C.

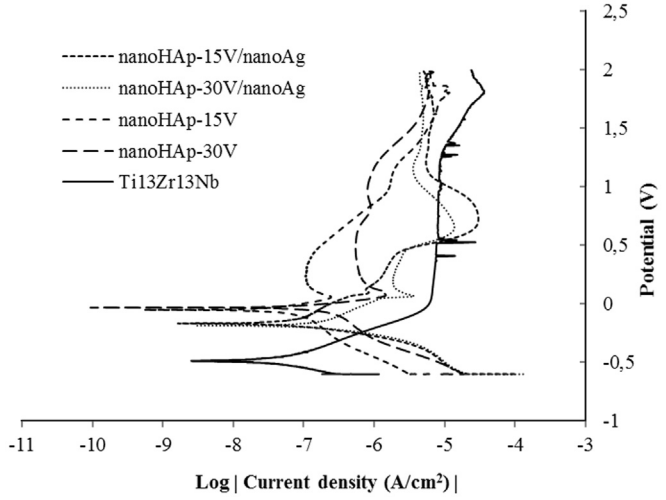

Fig. 7. Potentiodynamic polarization curves of nanoHAp coatings and reference specimen Ti13Zr13Nb in SBF at room temperature.

3.4. Corrosion properties

Fig. 7 and Table 3 illustrate the effect of the presence of nanoHAp deposits, both undecorated and decorated with nanoAg, on electrochemical behavior.

According to the results, titanium substrates with deposited nanoHAp coatings possess lower corrosion resistance as measured by corrosion current density. The corrosion resistance of titanium alloys with deposited nanoHAp was investigated and often proved greater than that of an uncoated substrate [29,66,67]. This means that the nanoHAp coatings obtained here promote corrosion, likely because of their slight thickness and porous structure, and, consequently, the presence of some corrosion channels and the appearance of localized corrosion. On the other hand, the corrosion rate is still at a minimal level.

The corrosion potentials, which were highest for the uncoated Ti13Zr13Nb reference sample, increased significantly for undecorated nanoHAp coatings. Mohan et al. reported a similar effect [52] for HAp/TiO_2 coatings on an Ti13Nb13Zr alloy, obtained by means of EPD. The shift of potentials to the anodic side means that nanoHAp coatings cause a shift of the anodic polarization curve to a positive direction.

Table 3
Corrosion current density and corrosion potential of the nanoHAp coatings and uncoated Ti13Zr13Nb substrate.

Sample	E_{corr} [V]	i_{corr} [nA/cm^2]
nanoHAp-15V coating	–0.046	72.54
nanoHAp-30V coating	–0.036	95.08
nanoHAp-15V/nanoAg	–0.462	7.21
nanoHAp-30V/nanoAg	–0.406	13.20
reference specimen Ti13Zr13Nb	–0.487	7.36

Table 4
Mechanical properties: hardness and Young's modulus of the nanoHAp-15V and nanoHAp-30V coatings.

Sample	Hardness (GPa)	Young's Modulus (GPa)
nanoHAp-15V coating	0.2245 ± 0.036	41.10 ± 8.91
nanoHAp-30V coating	0.0661 ± 0.008	19.52 ± 1.29

Table 5
Nanoindentation properties: maximum depth and plastic work of the nanoHAp-15V and nanoHAp-30V coatings.

Sample	Maximum depth (nm)	Plastic work (nj)	Elastic work (nj)
nanoHAp-15V coating	905.48 ± 74.04	1.17 ± 0.21	0.07 ± 0.01
nanoHAp-30V coating	1658.23 ± 98.08	2.54 ± 0.15	0.00 ± 0.01

Table 6
Nanoscratch test of the deposited nanoHAp-15V and nanoHAp-30V coatings.

Sample	Critical friction (mN)	Critical load (mN)
nanoHAp-15V coating	11.53 ± 2.23	35.83 ± 12.75
nanoHAp-30V coating	16.03 ± 1.41	66.43 ± 14.09

The addition of nanosilver particles reduces the corrosion current density. This effect is due to blocking of the pores by highly noble clusters. Investigations of silver-doped hydroxyapatite have been performed; however, either the investigated coatings were thick [68], or the hydroxyapatite coatings were deposited on TiO_2, which possesses excellent corrosion-resistant properties [65,68].

3.5. Nanoindentation and nanoscratch test

Table 4 shows the effect of deposition voltage on nanomechanical properties. A definite increase in hardness is observed with decreasing EPD voltage and decreasing thickness of nanoHAp coatings.

The nanoindentation values are in line with the plastic and elastic work shown in Table 5. At a doubled deposition voltage, the plastic work increases more than twofold. The value of elastic work appears negligible for both nanoHAp coatings. Probably the use of hydroxyapatite nanopowder and porous structure of nanoHAp coatings significantly reduced the hardness value and Young's modulus. The value of Young's modulus obtained here for nanoHAp-30V is similar to that achieved by Drevet et al. [17] using the EPD technique; greatly reduced hardness was observed in this study, presumably because of the more porous structure. There are some nanoindentation studies of nanohydroxyapatite coatings, for example performed by Dey et al. [69,70], Saber-Samandari et al. [71], Tang et al. [72]. However, the relatively thick coatings with larger grains as 20 nm were investigated. Saber-Samandari et al. showed the change of mechanical properties of coatings as related to the distance from the substrate. In other report, as the measurement depth increased, the investigated mechanical properties (hardness and Young's modulus) of the hydroxyapatite coating increased as well [73]. Polychronopoulou et al. [74] pointed out that nanoindentation measurements should be performed as close as possible to the surface top. The nanoindentation tests of nanohydroxyapatite coatings were presented by Drevet et al. [17], but thickness of these coatings was not measured. The relative values of Young's modulus obtained in the present study are similar to those reported by Drevet et al. [17], Fomin et al. [75] and Saber-Samandari et al.[73]. Young's modulus is a crucial parameter, as it ensures a

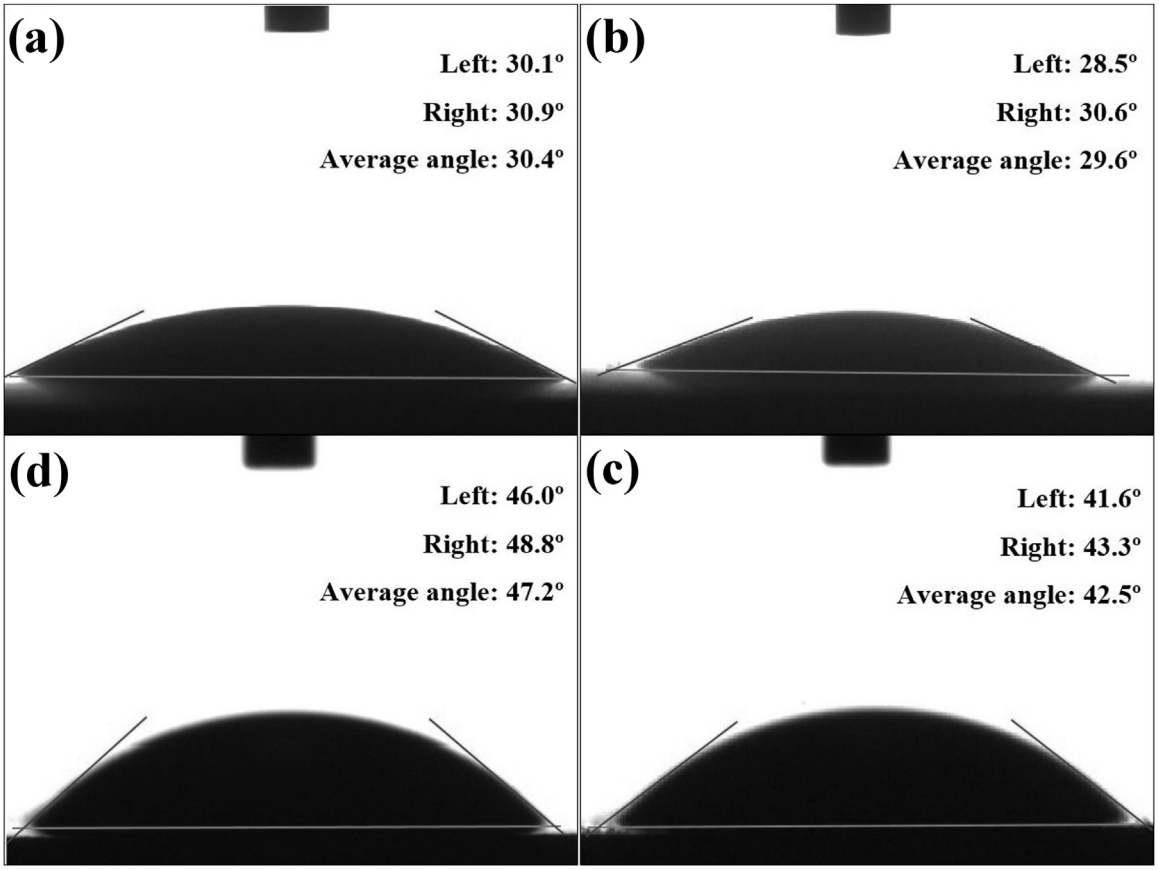

Fig. 8. Contact angle for water droplet on: (a) nanoHAp-15V, (b) nanoHAp-30V, (c) nanoHAp-15V/nanoAg, (d) nanoHAp-30V/nanoAg coatings.

strong connection between the implant and bone [17]. The Young's modulus of natural human bone (~20 GPa) [76] is very similar to that of nanoHAp-30V coatings. Moreover, poor mechanical properties cause the rapid dissolution of the coatings in a physiological environment [77].

The nanoscratch test results of nanoHAp-15V and nanoHAp-30V coatings are shown in Table 6. The initiation of coating delamination can be determined based on a sudden change in friction and normal forces. The increasing voltage results in critical friction higher by about 50% and a critical load higher by about 100%. Superior mechanical properties (lower value of hardness and Young's modulus) indicated the superior adhesion of the nanoHAp coating deposited on the Ti13Zr13Nb substrate. According to Kumar et al. [76], an increase in the adhesion strength of the coating to the substrate is due to higher values of fracture toughness, hardness, and elastic modulus.

3.6. Contact angle studies

The effect of deposition voltage on contact angle (Fig. 8) is slight because of the roughness values of both surfaces, which are not very different. The decoration of nanoHAp coatings with silver leads to a significant decrease in contact angle. It is well known that the wettability of metals is lower than that of polymers and ceramics; this is clearly shown in the presence of a relatively small amount of nanosilver, confirming the strong capability of metallic clusters to form van der Waals bonds.

The low contact angles for all specimens may be attributed to their porous surface structure. Contact angles are measures of wettability; their low values correspond to anticipated high biocompatibility. On the other hand, in [78] the best values of contact angle for cell attachment were assessed at 55° and for bone regeneration at 35° to 80° [78]; these values are higher than those recorded here.

The nanoHAp and nanoHAp/nanoAg coatings are regarded to be hydrophilic due to a large number of hydroxyl groups present on the surface [65]. An increasing thickness of the coating results also in an increasing crystallinity of the nanoHAp coating with hydrophilic hydroxyl groups as confirmed by the XRD studies [36]. With increasing EPD voltage, the thickness of the nanoHAp coatings increases as well. The thicker nanoHAp coating possesses more free space within its porous structure and larger number of cracks, which both reduce the value of contact angle. The presence of silver nanoparticles on the surface may, on the other hand, prevent the water droplets from penetrating the interior of the nanoHAp coating, resulting in an increase in the contact angle.

4. Conclusions

The electrophoretic deposition method, based on nanohydroxyapatite, performed within the short time of 1 min and followed by thermal treatment, yields thin, uniform, and rough surfaces with high values of mechanical properties, biocompatibility, and corrosion resistance.

The increase in deposition voltage, from 15 to 30 V, results in doubled thickness, improved adhesion and hardness, and comparable corrosion resistance and wettability.

The decoration of nanohydroxyapatite coatings with nanosilver leads to the achievement of protective silver concentration in artificial saliva after one or three days, depending on the nanoHAp deposition voltage, and will always exceed the upper limit of Ag concentration.

The nanohydroxyapatite coatings obtained by electrophoretic deposition at 30 V for 1 min, followed by thermal treatment at 800 °C for 120 min and decorated with nanosilver by means of reverse EPD at 60 V for 5 min, possess mechanical and chemical properties sufficient to permit their use as biocompatible, bioactive, and antibacterial coatings, in particular for dental screw implants.

References

[1] C. Oldani, A. Dominguez, Titanium as a biomaterial for implants, Recent Adv. Arthroplast. (2012) 149–162. http://dx.doi.org/10.5772/1445.

[2] S.S.A. El-Rahman, Neuropathology of aluminum toxicity in rats (glutamate and GABA impairment), Pharmacol. Res. 47 (2003) 189–194. http://dx.doi.org/10.1016/S1043-6618(02)00336-5.

[3] A. Smołka, G. Dercz, K. Rodak, B. Łosiewicz, Evaluation of corrosion resistance of nanotubular oxide layers on the Ti13Zr13Nb alloy in physiological saline solution / Ocena Odporności Korozyjnej Nanotubularnych Struktur Tlenkowych Na Stopie Ti13Zr13Nb W Środowisku Płynów Ustrojowych", Arch. Metall. Mater. 60 (2015) 8–13. http://dx.doi.org/10.1515/amm-2015-0432.

[4] L.M. Elias, S.G. Schneider, S. Schneider, H.M. Silva, F. Malvisi, Microstructural and mechanical characterization of biomedical Ti-Nb-Zr(-Ta) alloys, Mater. Sci. Eng. A 432 (2006) 108–112. http://dx.doi.org/10.1016/j.msea.2006.06.013.

[5] A. Zielinski, S. Sobieszczyk, T. Seramak, W. Serbinski, B. Swieczko-Zurek, A. Ossowska, Biocompatibility and bioactivity of load-bearing metallic implants, Adv. Mater. Sci. 10 (2011) 21–31. http://dx.doi.org/10.2478/v10077-010-0013-1.

[6] M. Geetha, A.K. Singh, R. Asokamani, A.K. Gogia, Ti based biomaterials, the ultimate choice for orthopaedic implants - a review, Progress. Mater. Sci. 54 (2009) 397–425. http://dx.doi.org/10.1016/j.pmatsci.2008.06.004.

[7] N. Eliaz, S. Shmueli, I. Shur, D. Benayahu, D. Aronov, G. Rosenman, The effect of surface treatment on the surface texture and contact angle of electrochemically deposited hydroxyapatite coating and on its interaction with bone-forming cells, Acta Biomater. 5 (2009) 3178–3191. http://dx.doi.org/10.1016/j.actbio.2009.04.005.

[8] M. Szklarska, G. Dercz, W. Simka, B. Łosiewicz, A.c. impedance study on the interfacial properties of passivated Ti13Zr13Nb alloy in physiological saline solution, Surf. Interface Anal. 46 (2014) 698–701. http://dx.doi.org/10.1002/sia.5383.

[9] S.F. Lamolle, M. Monjo, M. Rubert, H.J. Haugen, S.P. Lyngstadaas, J.E. Ellingsen, The effect of hydrofluoric acid treatment of titanium surface on nanostructural and chemical changes and the growth of MC3T3-E1 cells, Biomaterials 30 (2009) 736–742. http://dx.doi.org/10.1016/j.biomaterials.2008.10.052.

[10] J.W. Park, Y.J. Kim, J.H. Jang, T.G. Kwon, Y.C. Bae, J.Y. Suh, Effects of phosphoric acid treatment of titanium surfaces on surface properties, osteoblast response and removal of torque forces, Acta Biomater. 6 (2010) 1661–1670. http://dx.doi.org/10.1016/j.actbio.2009.10.011.

[11] A. Ossowska, S. Sobieszczyk, M. Supernak, A. Zielinski, Morphology and properties of nanotubular oxide layer on the "Ti-13Zr-13Nb" alloy, Surf. Coat. Technol. 258 (2014) 1239–1248. http://dx.doi.org/10.1016/j.surfcoat.2014.06.054.

[12] V. Dumas, A. Guignandon, L. Vico, C. Mauclair, X. Zapata, M.T. Linossier, W. Bouleftour, J. Granier, S. Peyroche, J.-C. Dumas, H. Zahouani, A. Rattner, Femtosecond laser nano/micro patterning of titanium influences mesenchymal stem cell adhesion and commitment, Biomed. Mater. 10 (2015) 55002. http://dx.doi.org/10.1088/1748-6041/10/5/055002.

[13] T.R. Rautray, R. Narayanan, K.H. Kim, Ion implantation of titanium based biomaterials, Progress. Mater. Sci. 56 (2011) 1137–1177. http://dx.doi.org/10.1016/j.pmatsci.2011.03.002.

[14] B. Majkowska, M. Jazdzewska, E. Wolowiec, W. Piekoszewski, L. Klimek, A. Zielinski, The possibility of use of laser-modified Ti6Al4V alloy in friction Pairs in endoprostheses, Arch. Metall. Mater. 60 (2015) 6–9. http://dx.doi.org/10.1515/amm-2015-0202.

[15] D. Wang, G. Wu, X. Lin, Y. Liu, Coatings for osseointegration of metallic biomaterials, Surf. Coat. Modif. Met. Biomater. (2015) 345–358. http://dx.doi.org/10.1016/B978-1-78242-303-4.00011-9.

[16] V. Ozhukil Kollath, Q. Chen, R. Closset, J. Luyten, K. Traina, S. Mullens, A.R. Boccaccini, R. Cloots, AC vs. DC electrophoretic deposition of hydroxyapatite on titanium, J. Eur. Ceram. Soc. 33 (2013) 2715–2721. http://dx.doi.org/10.1016/j.jeurceramsoc.2013.04.030.

[17] R. Drevet, N. Ben Jaber, J. Fauré, A. Tara, A. Ben Cheikh Larbi, H. Benhayoune, Electrophoretic deposition (EPD) of nano-hydroxyapatite coatings with improved mechanical properties on prosthetic Ti6Al4V substrates, Surf. Coat. Technol. 301 (2015) 94–99. http://dx.doi.org/10.1016/j.surfcoat.2015.12.058.

[18] A. Araghi, M.J. Hadianfard, Fabrication and characterization of functionally graded hydroxyapatite/TiO2 multilayer coating on Ti-6Al-4V titanium alloy for biomedical applications, Ceram. Int. 41 (2015) 12668–12679. http://dx.doi.org/10.1016/j.ceramint.2015.06.098.

[19] H. Farnoush, A. Sadeghi, A. Abdi Bastami, F. Moztarzadeh, J. Aghazadeh Mohandesi, An innovative fabrication of nano-HA coatings on Ti-CaP nanocomposite layer using a combination of friction stir processing and electrophoretic deposition, Ceram. Int. 39 (2013) 1477–1483. http://dx.doi.org/10.1016/j.ceramint.2012.07.092.

[20] H. Farnoush, J. Aghazadeh Mohandesi, D. Haghshenas Fatmehsari, F. Moztarzadeh, Modification of electrophoretically deposited nano-hydroxyapatite coatings by wire brushing on Ti-6Al-4V substrates, Ceram. Int. 38 (2012) 4885–4893. http://dx.doi.org/10.1016/j.ceramint.2012.02.079.

[21] K. Dudek, T. Goryczka, Electrophoretic deposition and characterization of thin hydroxyapatite coatings formed on the surface of NiTi shape memory alloy, Ceram. Int. 42 (2016) 19124–19132. http://dx.doi.org/10.1016/j.ceramint.2016.09.074.

[22] M. Bartmanski, A. Berk, A. Wojcik, The determinants of morphology and properties of the nanohydroxyapatite coating deposited on the Ti13Zr13Nb alloy by electrophoretic technique, Adv. Mater. Sci. 16 (2016) 56–66. http://dx.doi.org/10.1515/adms-2016-0017.

[23] H.J. Kim, Y.H. Jeong, H.C. Choe, W.A. Brantley, Surface characteristics of

hydroxyapatite coatings on nanotubular Ti-25Ta-xZr alloys prepared by electrochemical deposition, Surf. Coat. Technol. 259 (2014) 274–280. http://dx.doi.org/10.1016/j.surfcoat.2014.03.013.
[24] P. Strakowska, R. Beutner, M. Gnyba, A. Zielinski, D. Scharnweber, Electrochemically assisted deposition of hydroxyapatite on Ti6Al4V substrates covered by CVD diamond films - coating characterization and first cell biological results, Mater. Sci. Eng. C 59 (2016) 624–635. http://dx.doi.org/10.1016/j.msec.2015.10.063.
[25] Y. Huang, X. Zhang, H. Zhang, H. Qiao, X. Zhang, T. Jia, S. Han, Y. Gao, H. Xiao, H. Yang, Fabrication of silver- and strontium-doped hydroxyapatite/TiO2 nanotube bilayer coatings for enhancing bactericidal effect and osteoinductivity, Ceram. Int. 43 (2017) 992–1007. http://dx.doi.org/10.1016/j.ceramint.2016.10.031.
[26] Y. Huang, X. Zhang, H. Qiao, M. Hao, H. Zhang, Z. Xu, X. Zhang, X. Pang, H. Lin, Corrosion resistance and cytocompatibility studies of zinc-doped fluorohydroxyapatite nanocomposite coatings on titanium implant, Ceram. Int. 42 (2016) 1903–1915. http://dx.doi.org/10.1016/j.ceramint.2015.09.160.
[27] Y. Huang, Y. Yan, X. Pang, Electrolytic deposition of fluorine-doped hydroxyapatite/ZrO 2 films on titanium for biomedical applications, Ceram. Int. 39 (2013) 245–253. http://dx.doi.org/10.1016/j.ceramint.2012.06.017.
[28] B. Trybus, A. Zielinski, R. Beuter, T. Seramak, D. Scharnweber, Deposition of phosphate coatings on titanium within scaffold structure, Acta Bioeng. Biomech. (2016) 1–22. http://dx.doi.org/10.5277/ABB-00631-2016-03.
[29] P.C. Rath, L. Besra, B.P. Singh, S. Bhattacharjee, Titania/hydroxyapatite bi-layer coating on Ti metal by electrophoretic deposition: characterization and corrosion studies, Ceram. Int. 38 (2012) 3209–3216. http://dx.doi.org/10.1016/j.ceramint.2011.12.026.
[30] Y.E. Greish, A.S. Al Shamsi, K. Polychronopoulou, A.I. Ayesh, Structural evaluation, preliminary in vitro stability and electrochemical behavior of apatite coatings on Ti6Al4V substrates, Ceram. Int. 42 (2016) 18204–18214. http://dx.doi.org/10.1016/j.ceramint.2016.08.141.
[31] M. Badea, M. Braic, A. Kiss, M. Moga, E. Pozna, I. Pana, A. Vladescu, Influence of Ag content on the antibacterial properties of SiC doped hydroxyapatite coatings, Ceram. Int. 42 (2016) 1801–1811. http://dx.doi.org/10.1016/j.ceramint.2015.09.143.
[32] F.A. Azem, A. Kiss, I. Birlik, V. Braic, C. Luculescu, A. Vladescu, The corrosion and bioactivity behavior of SiC doped hydroxyapatite for dental applications, Ceram. Int. 40 (2014) 15881–15887. http://dx.doi.org/10.1016/j.ceramint.2014.07.116.
[33] D. Liu, K. Savino, M.Z. Yates, Coating of hydroxyapatite films on metal substrates by seeded hydrothermal deposition, Surf. Coat. Technol. 205 (2011) 3975–3986. http://dx.doi.org/10.1016/j.surfcoat.2011.02.008.
[34] K. Suchanek, A. Bartkowiak, A. Gdowik, M. Perzanowski, S. Kąc, B. Szaraniec, M. Suchanek, M. Marszałek, Crystalline hydroxyapatite coatings synthesized under hydrothermal conditions on modified titanium substrates, Mater. Sci. Eng. C 51 (2015) 57–63. http://dx.doi.org/10.1016/j.msec.2015.02.029.
[35] S. Mudenda, K.L. Streib, D. Adams, J.W. Mayer, R. Nemutudi, T.L. Alford, Effect of substrate patterning on hydroxyapatite sol-gel thin film growth, Thin Solid Films 519 (2011) 5603–5608. http://dx.doi.org/10.1016/j.tsf.2011.02.067.
[36] P. Usinskas, Z. Stankeviciute, A. Beganskiene, A. Kareiva, Sol-gel derived porous and hydrophilic calcium hydroxyapatite coating on modified titanium substrate, Surf. Coat. Technol. 307 (2016) 935–940. http://dx.doi.org/10.1016/j.surfcoat.2016.10.032.
[37] I.V. Pylypchuk, A.L. Petranovskaya, P.P. Gorbyk, A.M. Korduban, P.E. Markovsky, O.M. Ivasishin, Biomimetic hydroxyapatite growth on functionalized surfaces of Ti-6Al-4V and Ti-Zr-Nb alloys, Nanoscale Res. Lett. 10 (2015) 1–8. http://dx.doi.org/10.1186/s11671-015-1017-x.
[38] L. Guo, H. Li, Fabrication and characterization of thin nano-hydroxyapatite coatings on titanium, Surf. Coat. Technol. 185 (2004) 268–274. http://dx.doi.org/10.1016/j.surfcoat.2004.01.013.
[39] X. Pang, I. Zhitomirsky, Electrodeposition of hydroxyapatite-silver-chitosan nanocomposite coatings, Surf. Coat. Technol. 202 (2008) 3815–3821. http://dx.doi.org/10.1016/j.surfcoat.2008.01.022.
[40] X. Hu, H. Shen, Y. Cheng, X. Xiong, S. Wang, J. Fang, S. Wei, One-step modification of nano-hydroxyapatite coating on titanium surface by hydrothermal method, Surf. Coat. Technol. 205 (2010) 2000–2006. http://dx.doi.org/10.1016/j.surfcoat.2010.08.088.
[41] J. Xiong, Y. Li, P.D. Hodgson, C. Wen, Acta biomaterialia nanohydroxyapatite coating on a titanium – niobium alloy by a hydrothermal process, Acta Biomater. 6 (2010) 1584–1590. http://dx.doi.org/10.1016/j.actbio.2009.10.016.
[42] A. Bral, M.Y. Mommaerts, In vivo biofunctionalization of titanium patient-specific implants with nano hydroxyapatite and other nano calcium phosphate coatings: a systematic review, J. Cranio-Maxillofac. Surg. 44 (2016) 400–412. http://dx.doi.org/10.1016/j.jcms.2015.12.004.
[43] L.H. Lee, J.S. Ha, Deposition behavior and characteristics of hydroxyapatite coatings on Al2O3, Ti, and Ti6Al4V formed by a chemical bath method, Ceram. Int. 40 (2014) 5321–5326. http://dx.doi.org/10.1016/j.ceramint.2013.10.109.
[44] A. Mo, J. Liao, W. Xu, S. Xian, Y. Li, S. Bai, Preparation and antibacterial effect of silver-hydroxyapatite/titania nanocomposite thin film on titanium, Appl. Surf. Sci. 255 (2008) 435–438. http://dx.doi.org/10.1016/j.apsusc.2008.06.083.
[45] Y. Chen, X. Zheng, Y. Xie, H. Ji, C. Ding, H. Li, K. Dai, Silver release from silver-containing hydroxyapatite coatings, Surf. Coat. Technol. 205 (2010) 1892–1896. http://dx.doi.org/10.1016/j.surfcoat.2010.08.073.
[46] J. Qu, X. Lu, D. Li, Y. Ding, Y. Leng, J. Weng, S. Qu, B. Feng, F. Watari, Silver/hydroxyapatite composite coatings on porous titanium surfaces by sol-gel method, J. Biomed. Mater. Res. - Part B Appl. Biomater. 97 B (2011) 40–48. http://dx.doi.org/10.1002/jbm.b.31784.
[47] I.Y. Grubova, M.A. Surmeneva, A.A. Ivanova, K. Kravchuk, O. Prymak, M. Epple, V. Buck, R.A. Surmenev, The effect of patterned titanium substrates on the properties of silver-doped hydroxyapatite coatings, Surf. Coat. Technol. 276 (2015) 595–601. http://dx.doi.org/10.1016/j.surfcoat.2015.06.010.
[48] C. Fu, X. Zhang, K. Savino, P. Gabrys, Y. Gao, W. Chaimayo, B.L. Miller, M.Z. Yates, Antimicrobial silver-hydroxyapatite composite coatings through two-stage electrochemical synthesis, Surf. Coat. Technol. 301 (2016) 13–19. http://dx.doi.org/10.1016/j.surfcoat.2016.03.010.
[49] Z. Geng, R. Wang, X. Zhuo, Z. Li, Y. Huang, L. Ma, Z. Cui, S. Zhu, Y. Liang, Y. Liu, H. Bao, X. Li, Q. Huo, Z. Liu, X. Yang, Incorporation of silver and strontium in hydroxyapatite coating on titanium surface for enhanced antibacterial and biological properties, Mater. Sci. Eng. C 71 (2017) 852–861. http://dx.doi.org/10.1016/j.msec.2016.10.079.
[50] Y. Huang, M. Hao, X. Nian, H. Qiao, X. Zhang, X. Zhang, G. Song, J. Guo, X. Pang, H. Zhang, Strontium and copper co-substituted hydroxyapatite-based coatings with improved antibacterial activity and cytocompatibility fabricated by electrodeposition, Ceram. Int. 42 (2016) 11876–11888. http://dx.doi.org/10.1016/j.ceramint.2016.04.110.
[51] F. Technique, R. Metals, T. Alloys, T. Alloys, Q. Program, Standard Specification for Wrought Titanium-13Niobium-13Zirconium Alloy for Surgical Implant Applications (UNS R58130) 1Annual Book of ASTM Standards (2011), 2011, pp. 4–8. http://dx.doi.org/10.1520/F1713-08.2.
[52] L. Mohan, D. Durgalakshmi, M. Geetha, T.S.N. Sankara Narayanan, R. Asokamani, Electrophoretic deposition of nanocomposite (HAp + TiO 2) on titanium alloy for biomedical applications, Ceram. Int. 38 (2012) 3435–3443. http://dx.doi.org/10.1016/j.ceramint.2011.12.056.
[53] J. Loch, H. Krawiec, Corrosion behaviour of cobalt alloys in artifical salvia solution, Arch. Foundry Eng. 13 (2013) 101–106.
[54] A. Tahmasbi Rad, M. Solati-Hashjin, N.A.A. Osman, S. Faghihi, Improved biophysical performance of hydroxyapatite coatings obtained by electrophoretic deposition at dynamic voltage, Ceram. Int. 40 (2014) 12681–12691. http://dx.doi.org/10.1016/j.ceramint.2014.04.116.
[55] R. Boccaccini, S. Keim, R. Ma, Y. Li, I. Zhitomirsky, Electrophoretic deposition of biomaterials, J. R. Soc., Interface / R. Soc. 7 (2010) 581–613. http://dx.doi.org/10.1098/rsif.2010.0156.focus.
[56] M. Farrokhi-Rad, T. Shahrabi, Effect of suspension medium on the electrophoretic deposition of hydroxyapatite nanoparticles and properties of obtained coatings, Ceram. Int. 40 (2014) 3031–3039. http://dx.doi.org/10.1016/j.ceramint.2013.10.004.
[57] A.A. Abdeltawab, M.A. Shoeib, S.G. Mohamed, Electrophoretic deposition of hydroxyapatite coatings on titanium from dimethylformamide suspensions, Surf. Coat. Technol. 206 (2011) 43–50. http://dx.doi.org/10.1016/j.surfcoat.2011.06.034.
[58] B. Feng, J. Weng, B.C. Yang, S.X. Qu, X.D. Zhang, Characterization of surface oxide films on titanium and adhesion of osteoblast, Biomaterials 24 (2003) 4663–4670. http://dx.doi.org/10.1016/S0142-9612(03)00366-1.
[59] K.A. Gross, M. Babovic, Influence of abrasion on the surface characteristics of thermally sprayed hydroxyapatite coatings, Biomaterials 23 (2002) 4731–4737. http://dx.doi.org/10.1016/S0142-9612(02)00222-3.
[60] B.D. Boyan, T.W. Hummert, D.D. Dean, Z. Schwartz, Role of material surfaces in regulating bone and cartilage cell response, Biomaterials 17 (1996) 137–146. http://dx.doi.org/10.1016/0142-9612(96)85758-9.
[61] X. Chen, H.J. Schluesener, Nanosilver: a nanoproduct in medical application, Toxicol. Lett. (2008). http://dx.doi.org/10.1016/j.toxlet.2007.10.004.
[62] W. Lesniak, A.U. Blelinska, K. Sun, K.W. Janczak, X. Shi, J.R. Baker, L.P. Balogh, Silver/dendrimer nanocomposites as biomarkers: fabrication, characterization, in vitro toxicity, and intracellular detection, Nano Lett. 5 (2005) 2123–2130. http://dx.doi.org/10.1021/nl051077u.
[63] B. Reidy, A. Haase, A. Luch, K.A. Dawson, I. Lynch, Mechanisms of silver nanoparticle release, transformation and toxicity: a critical review of current knowledge and recommendations for future studies and applications, Materials 6 (2013) 2295–2350. http://dx.doi.org/10.3390/ma6062295.
[64] R.D. Glover, J.M. Miller, J.E. Hutchison, Generation of metal nanoparticles from silver and copper objects: nanoparticle dynamics on surfaces and potential sources of nanoparticles in the environment, ACS Nano 5 (2011) 8950–8957. http://dx.doi.org/10.1021/nn2031319.
[65] M. Mirzaee, M. Vaezi, Y. Palizdar, Synthesis and characterization of silver doped hydroxyapatite nanocomposite coatings and evaluation of their antibacterial and corrosion resistance properties in simulated body fluid, Mater. Sci. Eng. C 69 (2016) 675–684. http://dx.doi.org/10.1016/j.msec.2016.07.057.
[66] C.T. Kwok, P.K. Wong, F.T. Cheng, H.C. Man, Characterization and corrosion behavior of hydroxyapatite coatings on Ti6Al4V fabricated by electrophoretic deposition, Appl. Surf. Sci. 255 (2009) 6736–6744. http://dx.doi.org/10.1016/j.apsusc.2009.02.086.
[67] M. Sankar, S. Suwas, S. Balasubramanian, G. Manivasagam, Surface & coatings technology comparison of electrochemical behavior of hydroxyapatite coated onto WE43 Mg alloy by electrophoretic and pulsed laser deposition, SCT 309 (2017) 840–848. http://dx.doi.org/10.1016/j.surfcoat.2016.10.077.
[68] Y. Yan, X. Zhang, Y. Huang, Q. Ding, X. Pang, Antibacterial and bioactivity of silver substituted hydroxyapatite/TiO2 nanotube composite coatings on titanium, Appl. Surf. Sci. 314 (2014) 348–357. http://dx.doi.org/10.1016/j.apsusc.2014.07.027.
[69] A. Dey, A.K. Mukhopadhyay, S. Gangadharan, M.K. Sinha, D. Basu, N.R. Bandyopadhyay, Nanoindentation study of microplasma sprayed hydroxyapatite coating, Ceram. Int. 35 (2009) 2295–2304. http://dx.doi.org/10.1016/j.ceramint.2009.01.002.
[70] A. Dey, A.K. Mukhopadhyay, Evaluation of residual stress in microplasma sprayed hydroxyapatite coating by nanoindentation, Ceram. Int. 40 (2014) 1263–1272.

http://dx.doi.org/10.1016/j.ceramint.2013.06.073.
[71] S. Saber-Samandari, K.A. Gross, Nanoindentation on the surface of thermally sprayed coatings, Surf. Coat. Technol. 203 (2009) 3516–3520. http://dx.doi.org/10.1016/j.surfcoat.2009.05.033.
[72] C.Y. Tang, P.S. Uskokovic, C.P. Tsui, D. Veljovic, R. Petrovic, D. Janackovic, Influence of microstructure and phase composition on the nanoindentation characterization of bioceramic materials based on hydroxyapatite, Ceram. Int. 35 (2009) 2171–2178. http://dx.doi.org/10.1016/j.ceramint.2008.11.028.
[73] S. Saber-Samandari, K.A. Gross, Nanoindentation reveals mechanical properties within thermally sprayed hydroxyapatite coatings, Surf. Coat. Technol. 203 (2009) 1660–1664. http://dx.doi.org/10.1016/j.surfcoat.2008.12.025.
[74] K. Polychronopoulou, C. Rebholz, M.A. Baker, L. Theodorou, N.G. Demas, S.J. Hinder, A.A. Polycarpou, C.C. Doumanidis, K. Böbel, Nanostructure, mechanical and tribological properties of reactive magnetron sputtered TiCx coatings, Diam. Relat. Mater. 17 (2008) 2054–2061. http://dx.doi.org/10.1016/j.diamond.2008.07.007.
[75] A. Fomin, M. Fomina, V. Koshuro, I. Rodionov, A. Zakharevich, A. Skaptsov, Structure and mechanical properties of hydroxyapatite coatings produced on titanium using plasma spraying with induction preheating, Ceram. Int. (2017) 0–1. http://dx.doi.org/10.1016/j.ceramint.2017.05.168.
[76] R.M. Kumar, K. Kumar, S. Singh, P. Gupta, B. Bhushan, P. Gopinath, D. Lahiri, Surface and coatings technology electrophoretic deposition of hydroxyapatite coating on Mg – 3Zn alloy for orthopaedic application, Surf. Coat. Technol. 287 (2016) 82–92. http://dx.doi.org/10.1016/j.surfcoat.2015.12.086.
[77] L. Clèries, J. Fernández-Pradas, J. Morenza, Behavior in simulated body fluid of calcium phosphate coatings obtained by laser ablation, Biomaterials 21 (2000) 1861–1865. http://dx.doi.org/10.1016/S0142-9612(00)00060-0.
[78] S. Heise, M. Höhlinger, Y. Torres, J. José, P. Palacio, J. Antonio, R. Ortiz, V. Wagener, S. Virtanen, A.R. Boccaccini, Electrochimica acta electrophoretic deposition and characterization of chitosan / bioactive glass composite coatings on Mg alloy substrates, Electrochim. Acta 232 (2017) 456–464. http://dx.doi.org/10.1016/j.electacta.2017.02.081.